International Journal of Engineering Research-Online
A Peer Reviewed International Journal
Articles available online http://www.ijoer.in; editorijoer@gmail.com

Vol.5., Issue.3, 2017
May-June

RESEARCH ARTICLE

ISSN: 2321-7758

A Double Bow-Tie Slot Antenna With and Without Circular Patch for Terahertz Applications

DEEPIKA P[1], GEETHA P[2]
[1]Communication Systems, P.R.Engineering College Vallam, Thanjavur Tamilnadu.
email:pdeepikaece03@gmail.com
[2]Asst. Professor, ECE P.R. Engineering College Vallam, Thanjavur Tamilnadu.
email:geethakarthy@gmail.com.

ABSTRACT
This paper presents millimetre-wave and terahertz double bow-tie slot antennas. Two different antennas are designed to cover 0.1–0.3 and 0.2– 0.4 THz, respectively. The double bow-tie slot antenna results in a wide impedance bandwidth and 78–97% Gaussian coupling efficiency over a 3:1 frequency range. Absolute gain measurements done at 100–400 GHz and 100– 350 GHz confirm the wideband operation of this design. The double bow-tie slot antenna is intended to fill the gap between standard double-slot antennas and log periodic and sinuous antennas, with applications areas in radio astronomy and imaging systems.

Key Words—Bow-tie slot antenna, millimetre-wave antennas, radio-frequency (RF) filters, self-complementary antennas, slot antenna, terahertz antennas.

.

I. INTRODUCTION

Double-Slot and slot-ring antennas on a quartz and silicon dielectric lenses have been extensively used for planar millimeter-wave and terahertz applications, with applications in radio astronomy, communication systems, and low-power radars. They offer symmetrical patterns into the dielectric lens, which transfers to a high Gaussian-beam coupling efficiency in a quasi-optical system. Also, they do not support substrate modes and have a low cross-polarization level (< −20 dB) and their geometry allows for a dual-polarization design. The effect of the dielectric lens-to-air interface was also extensively studied versus the extension length. Also, the reflections inside the lens on the far-field patterns and antenna impedance can now be accurately simulated using Ansys-HFSS and are now taken into account in the design procedure of high-performance receivers.

The double-slot antenna naturally focuses the energy to the center of the double-slot and a detector is placed at this position. A low-pass filter is, therefore, required at the edge of one of the slot antennas to allow for biasing of the detector and for dc and IF signals. It allows for a symmetrical field distribution between the two slot antennas, and a symmetrical pattern in the far field.

One drawback of the standard double-slot antenna is its relatively narrow impedance and pattern bandwidth. The antennas can operate well over a ± 20% bandwidth, and while this is acceptable for a large set of applications, it is not acceptable for octave or multioctave operations.

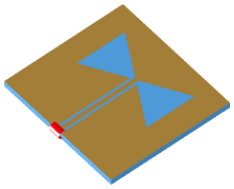

Fig 1: Model double slot bow tie antenna

In this case, a self-complementary antenna is used such as log-periodic, spiral, or sinuous antennas. These antennas can cover a 10:1

frequency range with a near constant impedance on a dielectric lens, and have a natural radio-frequency (RF) filter between the detector placed at the center and the dc (or low IF) taken from the edges. Also, single and dual polarized designs can be built using such antennas. However, they do not have the polarization purity as double-slot antennas or the ability to control the antenna impedance for a variety of different detectors. Nevertheless, frequency-independent self-complementary antennas are appealing in wideband applications since their bandwidth is determined only by their dimensions. Dual-polarized leaky wave antennas are also presented for broadband terahertz applications. These antennas are technologically challenging to build due to the use of large thin membranes.

Recently, a double-slot antenna with improved butterfly-shaped design showed a 2:1 response at 0.6–1.2 THz. In this design, the width of the slot dipoles is substantially increased to achieve wideband performance. However, the impedance and radiation patterns of this antenna have not been thoroughly analyzed on dielectric lenses.

This paper presents a double bow-tie slot antenna for wide-band applications, with a frequency range of approximately 3:1.

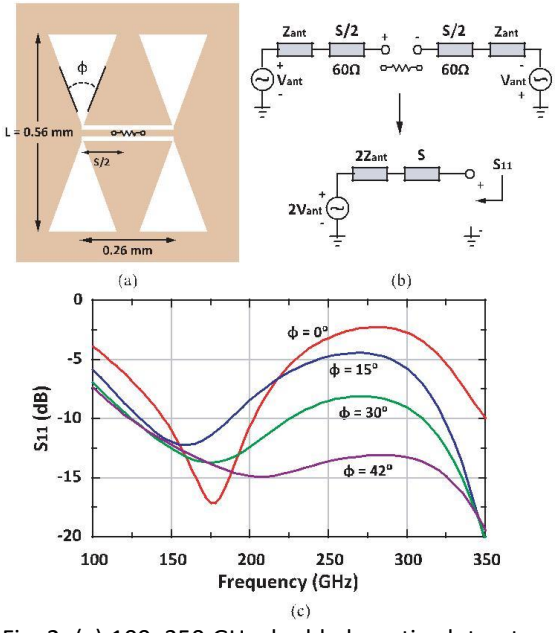

Fig. 2. (a) 100–350 GHz double bow-tie slot antenna layout, (b) design schematic, and (c) antenna return loss versus different bow-tie angles (ϕ) with Zin = 100 Ω.

The work is intended to fill the gap between the double-slot antenna and the ultrawideband complementary antennas. The design and measurements of a double bow-tie slot antenna placed on a synthesized elliptical silicon dielectric lens is presented at 100–350 GHz and at 100–400 GHz with good performance.

II. DESIGN AND SIMULATIONS

The double bow-tie slot antenna is presented in Fig. 1. There are three essential design criteria, which are required for wideband operation and these are: 1) wideband impedance at the detector ports; 2) a low-pass filter capable of operating at millimetre wave frequencies and presenting a low impedance to the slot-antenna feed point over a 3:1 frequency range; and 3) wideband and symmetrical pat-terns with low cross-polarization levels and capable of a high Gaussian-beam coupling efficiency. The wideband low-pass filter rejects any RF power leaking out of the double bow-tie slot antenna and increases the antenna efficiency.

A. Impedance

The double bow-tie slot antenna geometry is first optimized. Assuming a perfect short at both antennas as shown in Fig. 2. Several bow-tie angles were considered starting from $\varphi = 0^{\circ}$ (standard double slot) to $\varphi = 45^{\circ}$. Note that the maximum allowed angle before the edges touch each other is $\varphi \approx 55^{\circ}$. The separation between the bow-tie antennas is 0.17 λ_o at 200 GHz (100– 300 GHz operation), which is a compromise between pattern degradation versus frequency and antenna impedance. A larger separation allows for wider bow-tie angles and less impedance variation, but results in rapid pattern degradation at the higher edge of the operating band. A smaller separation has larger mutual coupling between the two slot antennas and also smaller bow-tie angles, and this results in more variation in the antenna impedance.

The double bow-tie slot antenna is designed at a centre frequency (f_o) of 200 GHz with L = 0.56 mm, S = 0.26 mm, and $\varphi = 42^{\circ}$. The 200–600 GHz antenna is designed for f_o = 400 GHz with L = 0.28 mm and S = 0.136 mm. The simulated input impedance of different bow-tie antennas versus frequency is shown in Fig. 2(c). Simulations are done using ADS-Momentum on a dielectric half-space

with (ε_r = 11.7), and do not take into account any lens reflections. The bow-tie slot antennas operate near their second resonance point due to their inherent wideband operation at this length. Note that slot antennas with an angle of φ = 20 − 45° are much more wideband than the standard φ = 0° design. The mutual coupling (Z_{12}) is taken into account in the driving point impedance of each antenna as $Z_{ant} = Z_{11} - Z_{12}$, and a transmission-line section of Z_o = 60 Ω is used between the antennas and the detector for wideband matching. The impedance match is < −10 dB at 120–350 GHz for a differential load of 100 Ω. In this design, the detector impedance is chosen to be 100 Ω, but other detector impedances can be used and the matching network reoptimized.

B. Wideband Low-Pass Filter

B. Wideband Low-Pass Filter

The low-pass filter is an essential component in the design and must have high rejection over the full operating band since it should present a short to the slot-antenna feed. The standard high-Z/low-Z impedance filter, which is commonly used is narrowband with a maximum rejection of 20–25 dB and a second passband at ≈ $3f_0$, where f_0 is the 3-dB cutoff frequency of the filter. Therefore, a complex miniature multisection coplanar-waveguide (CPW) periodic filter has been designed and simulated using ADS-Momentum. The filter is based on a slow-wave propagation design, which is accomplished by effectively increasing the transmission-line *L* and *C* values. This is achieved by changing the CPW line width to control the inductance per unit length and changing the space between the signal lines and the ground to control the capacitance. The overall footprint of the periodic structures remains the same compared to a standard 50 Ω CPW line. Three CPW unit cells are designed to reject signals at 100–300 GHz, and each unit-cell length is determined by its cutoff frequency f_c with

$$l1,2,3 = \frac{c0}{\sqrt{\xi effz}\,2fc1,2,3} \quad (\xi eff = 6.5)$$

The length of each unit cell is optimized such that l_1 = 0.27 mm, l_2 = 0.25 mm, and l_3 = 0.22 mm and $f_{c\,1}$, $f_{c\,2}$, $f_{c\,3}$ = 220, 238, 270 GHz, respectively. The simulated S-parameters show a rejection >20 dB at 110–320 GHz with an insertion loss <0.5 dB up to 50 GHz. The filter is 0.78 mm long with line widths and slot width varying between 3.5 and 18.5 μm and is compatible with standard lithography. The impedance seen from the bow-tie slot antenna is <1−j50 Ω at 115–280 GHz. The RF low-pass filter for the 300–600 GHz antenna has nearly the same performance (S_{21} < −20 dB) and is not shown for brevity. These filters exhibit low insertion loss and simple fabrication

C. Radiation Patterns

The simulated patterns inside the dielectric lens for the double bow-tie antenna with $L = 0.37\lambda_o$ and $S = 0.17\lambda_o$ at 200 GHz are shown in Fig. 4. Again, these patterns are simulated on a semi-infinite substrate using ADS-Momentum. The cross-polarization component is <−40 dB in the principal planes and remains <−20 dB at 100–300 GHz in the diagonal planes. The power radiated to the backside is < 6% over the frequency range. These patterns are similar to double-slot antennas with φ = 0° (standard design).A better way to look at the pattern is to study the far-field patterns when the double bow-tie slot antenna is placed at the hyperhemispherical point with $L_{ext} = R_{lens}/n$, where L_{ext} is the extended length, R_{lens} is the lens radius, and *n* is the silicon index of refraction (≈3.42). At the hyperhemi-spherical position, the directivity increases by n^2 and at the synthesized elliptical position (L_{ext} = 0.33−0.38 R_{lens}), the antenna becomes diffraction limited with

$$D = \frac{4\pi\varepsilon_{ap} A_P}{\lambda^2 \; o}$$

where AP is the lens physical area (πR2lens /4) and εap is the aperture efficiency.

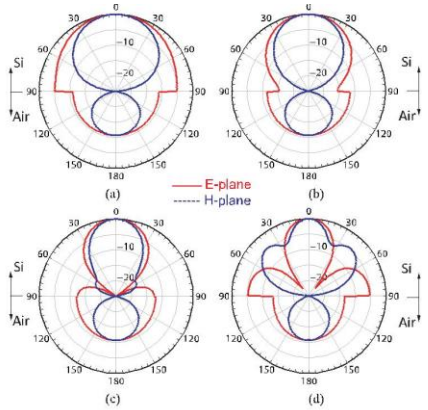

Fig. 4. Simulated radiation pattern at: (a) 125 GHz, (b) 175 GHz, (c) 225 GHz, and 275 GHz.

For a lens radius of 6 mm, the elliptical position is achieved with Lext = 0.34Rlens and the far-field patterns are simulated us-ing Ansys-HFSS. A comparison between the antenna directivity at different lens positions and the aperture efficiency and Gaussian coupling efficiency at the synthesized elliptical position are presented. The Gaussian beam calculations are done using

$$E_{|\text{Gaussian}|}(\theta) = e^{-(\theta/\theta_e)^2}.$$

The Gaussian coupling efficiency and aperture efficiency are 78–97% and 55–87% at 100–300 GHz, respectively. The degradation in aperture efficiency at 300 GHz is due to the directive and non-symmetrical patterns inside the silicon lens. Note that the double bow-tie slot antenna results in very similar values as the standard double-slot antenna.

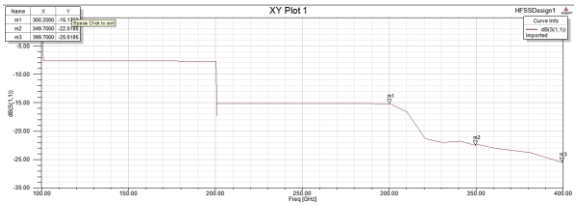

Fig. 5. Simulated S parameter of double bow tie antenna with circular patch

III. MEASUREMENTS

A. Impedance

A scaled double bow-tie slot antenna model with f_o = 8 GHz was fabricated on a 20 mil thick Rogers 3 010/6 010 substrate (ε_r = 10.7, tan δ = 0.0023 at 10 GHz) with L = 40 mm and S = 25 mm, and placed on a 10-cm silicon lens. The low-pass filter was not present and a coaxial-feed was soldered to the two antenna feeds. The measurements at 2–14 GHz are done using an open-short calibration at the coaxial-line tips (no load is used) since the coaxial line is physically short, and the measured impedance is referenced to the antenna ports. Also, time domain was used to remove the multiple reflections from the silicon–air interface. The two coaxial lines were fed into a differential vector network analyzer to measure S_{11} . The measured input impedance is equivalent to 2 $\times(Z_{11}–Z_{12}$) and agrees well with simulations with a wide-band operation from 2–14 GHz.

B. Wideband CPW Low-Pass Filter

The CPW low-pass filter was fabricated on a high resistivity silicon substrate (ε_r = 11.7, ρ > 7 kΩ · cm) with a 0.2 μm SiO_2 layer. A sputtered gold layer (0.3 μm) with additional electroplated gold (2–3 μm) on some areas was used. Air bridges with l = 125 μm and w = 20 μm were placed every 80–120 μm over the filter to equalize the CPW grounds, and their capacitance was taken in the filter design. The filter S-parameters are measured using an Agilent vector network analyzer on a probe station with SOLT calibration (short-open-line-thru) to the GSG pads. The measured filter response shows a wideband rejection ≥20 dB at 100–220 GHz (max. range), but the insertion loss is higher than simulated and is 1.5 dB at 10 GHz. We believe that this is due to charges created at the SiO_2 /silicon interface in the CPW gaps, which greatly increase the transmission-line loss.

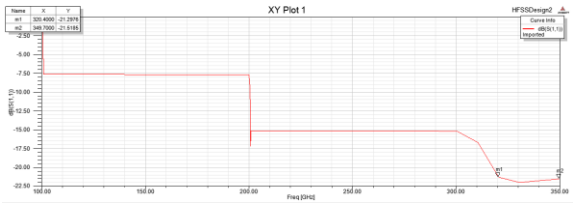

Fig. 6. Simulated S parameter of double bow tie antenna without circular patch

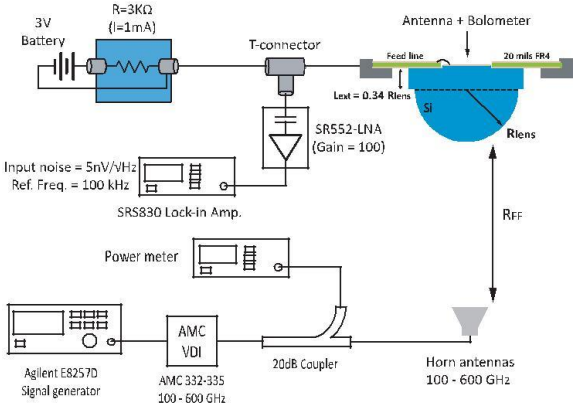

Fig. 7. Double bow-tie slot antenna measurement setup.

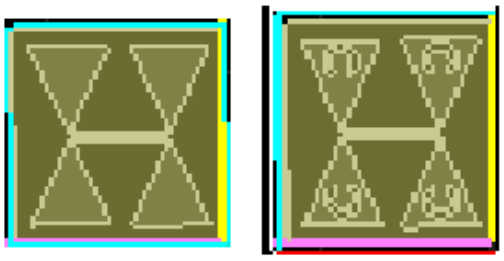

Fig. 8 hardware model of double bow tie slot antenna with and without circular patch

The filter is well matched with S_{11} < −20 dB. Since the filter is symmetrical, S_{22} and S_{12} are not shown for brevity.

C. Radiation Patterns

Two double bow-tie slot antennas were fabricated on a high-resistivity silicon substrate using sputtered and electro-plated gold layers. One design was centered at 200 GHz (100– 300 GHz) and another design was centered at 400 GHz (200– 600 GHz). A nickel/chrome microbolometer detector with a size of 3 μm (width) × 30 μm (length) × 25 nm (thickness), an impedance of 60–120 Ω (different fabrication lots) and a responsivity of 15–35 V/W was used. To avoid the thermal loss to the substrate and maximize the responsivity, an air-suspended bolometer structure was used.

The 100–300 GHz antenna was placed on a silicon lens with R_{lens} = 6 mm and a 525 μm high-resistivity silicon wafer was used between the hyper hemispherical lens (L_{ext} = 1.1 mm) and the silicon substrate containing the antenna (400 μm thick) so as to place the antenna at the synthesized elliptical position (L_{ext} = 0.34 R_{lens}). The 200–600 GHz was placed on a silicon lens with R_{lens} = 3 mm and a 200 μm high-resistivity silicon wafer was used between the hyper hemispherical lens (L_{ext} = 0.45 mm) and the silicon substrate containing the antenna (400 μm thick) so as to also place the antenna at the synthesized elliptical position. The alignment was done by hand using a fine manipulator on a far-field stage until the pattern was centered, and then, the lens was glued and not changed anymore. No λ_m /4 matching layer is used on the silicon lens, and all measurements include the silicon–air interf5xace reflections. The measurement setup is shown in Fig. 8. A selection of horn antennas and AMC-VDI multiplier chains are used to cover 100–500 GHz. The distance (R_{FF}) between the two antennas is always larger than the far-field condition ($2D^2/\lambda$) where D is the diameter of the largest antenna. For the 100–300 GHz design, R_{FF} is chosen to be 30 cm. For the 200–600 GHz design, R_{FF} is 18 cm.

The measured and simulated radiation patterns are shown in Fig. 9 for the 100–300 GHz design. Due to the mechanical mount, the pattern could only be measured to ±25°, but this was enough to check the pattern shape and symmetry. At 125 GHz, the patterns are relatively broad due to the small lens size ($5\lambda_o$), and at 275 GHz, the patterns start becoming unsymmetrical due to the feed pattern inside the lens. The 3 dB beam width for the E and H planes are shown in Fig. 10 and the measurements agree well with simulations. A comparison between the measured patterns at 225 GHz and a filled Gaussian beam, with Gaussian coupling efficiency >97%.

Since the patterns are measured only in two principle planes (φ = 0°, 90°), a comparison between the simulated and measured directivity is done by extracting it from both simulations and measurements with

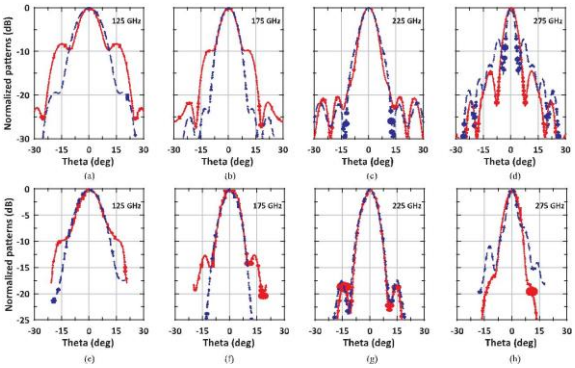

Fig. 9. Simulated [(a)–(c) and (f)] and measured [(d)–(f) and (i)] radiation patterns. (Solid: E plane, dashed: H plane).

$$D = \frac{32400}{\phi_{3dB\text{-}E}\ \phi_{3dB\text{-}H}}$$

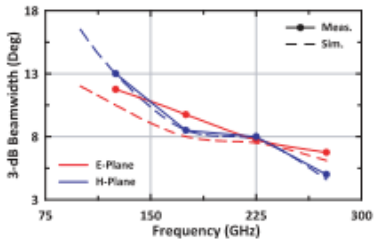

Fig. 10. Measured and simulated 3-dB beamwidths for the E and H planes (R_{lens} = 6 mm).

The measured directivity is 23–30 dB at 125–275 GHz. The patterns for the 200–600 GHz antenna are shown in Fig. 13 and show similar directivity as the 100–300 GHz antenna. For both antennas, the cross-polarization component could not be measured in the principal planes and was < −30 dB at all frequencies.

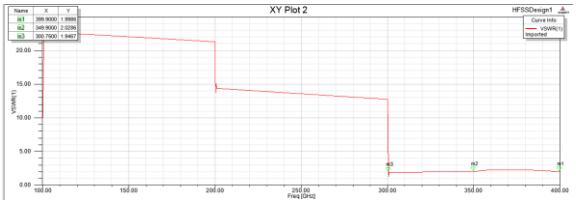

Fig. 11 Simulated VSWR of double bow tie slot antenna with circular patch

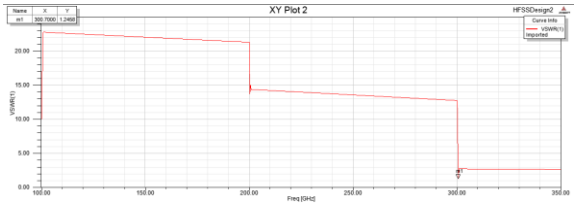

Fig. 12 Simulated VSWR of double bow tie slot antenna without circular patch

D. Absolute Gain Measurements

A direct way to measure the wideband properties of the double bow-tie slot antenna is to measure its absolute gain versus frequency. The power received at the detector (PR) is calculated using the Friis transmission formula [29] as

$$P_R = P_T G_T G_R \left(\frac{\lambda}{4\pi R}\right)^2$$

where P_T and G_T are the transmit power and transmit horn gain and are calibrated independently. The double bow-tie slot antenna gain, G_R , is calculated as

$$G_R = \varepsilon_{br}\, \varepsilon_{sloss}\, \varepsilon_{refl}\, (1 - |\Gamma|)^2\, D_R$$

where D_R is the front-pattern directivity obtained using HFSS, ε_{br} is the back-side power loss (0.3–0.4 dB at 100–350 GHz), ε_{sloss} is the silicon lens absorption loss (0.2 dB), ε_{refl} is the silicon-to-air reflection loss (≈1.7 dB), and Γ is the antenna-detector impedance mismatch.

In the measurement setup the source is square-wave AM modulated at 1 kHz, which is well within the microbolometer detector thermal frequency response. The detector has a measured responsivity of 18.5 and 31.5 V/W for the 200 and 400 GHz designs, respectively. Measurements are done at 1 mA of bias current, and the detected voltage is measured using a lock-in amplifier. At 100–400 GHz, P_T = 0.5–1 mW, G_T = 21–26 dB, R_{FF} = 20–35 cm depends on the size of the lens, and the measured voltage from the detector is 40–80 μV corresponding to 1.26–4.32 μW of received power.

The receiver antenna gain (G_R) can be accurately obtained using the detector voltage and the aforementioned equations, and is plotted in Fig. 12 and 14. The effect of the mismatch between the antenna impedance and the bolometer resistance is taken out of the gain calculations. As can be seen, G_R agrees well with simulations over a wide frequency range, showing that this antenna is wideband in pattern and impedance. The ripples in the measured gain are due to the absence of a wide-band matching layer, and standing waves in the measurement system.

IV. CONCLUSION

Two double bow-tie slot antennas are shown to cover a range frequency range of 100–300 and 200–600 GHz for millimeter-wave and terahertz applications. The use of a bow-tie slot sig-nificantly increases the impedance bandwidth, and a new design for the low-pass filter ensures a wideband short over a 3:1 fre-quency range. This antenna should find applications in radio-astronomical systems or terahertz imaging systems required a 3:1 frequency range.

ACKNOWLEDGMENT

The authors would like to thank the staff of the San Diego Nano3 Laboratory, University of California, for their support during the antenna fabrication.

REFERENCES

[1] J. Zmuidzinas, “Quasioptical slot antenna SIS mixers,” IEEE Trans. Mi-crow. Theory Techn., vol. 40, no. 9, pp. 1797–1804, Sep. 1992.

[2] G. Chattopadhyay and J. Zmuidzinas, “A dual-polarized slot antenna for millimeter waves,” IEEE Trans. Antennas Propag., vol. 46, no. 5, pp. 736– 737, May 1998.

[3] D. Filipovic, S. Gearhart, and G. M. Rebeiz, “Double-slot antennas on ex-tended hemispherical and elliptical silicon dielectric lenses,” IEEE Trans. Microw. Theory Techn., vol. 41, no. 10, pp. 1738–1749, Oct. 1993.

[4] S. Gearhart and G. M. Rebeiz, “A monolithic 250 GHz Schottky-diode receiver,” IEEE Trans. Microw. Theory Techn., vol. 42, no. 12, pp. 2504– 2511, Dec. 1994.

[5] M. V. der Vorst et al., “Effect of internal reflections on the radiation properties and input impedance of integrated lens antennas —Comparison between theory and measurements,” IEEE Trans. Microw. Theory Techn., vol. 49, no. 6, pp. 1118–1125, Jun. 2001.

[6] A. Neto, S. Maci, and P. J. I. de Maagt, “Reflections inside an elliptical dielectric lens antenna,” Proc. IEEE, vol. 145, no. 3, pp. 243–247, Jun. 1998.

[7] A. Neto, "UWB, non dispersive radiation from the planarly fed leaky lens antenna—Part 1: Theory and design," IEEE Trans. Antennas Propag., vol. 58, no. 7, pp. 2238–2247, Jul. 2010.

[8] Y. Mushiake, "Self-complementary antennas," IEEE Antennas Propag. Mag., vol. 34, no. 6, pp. 23–29, Dec. 1992.

[9] B. K. Kormanyos, P. H. Ostdiek, W. L. Bishop, T. W. Crowe, and G. M. Rebeiz, "A planar wideband 80–200 GHz subharmonic receiver," IEEE Trans. Microw. Theory Techn., vol. 41, no. 10, pp. 1730–1737, Oct. 1993.

[10] A. Semenov et al., "Terahertz performance of integrated lens anten-nas with a hot-electron bolometer," IEEE Trans. Microw. Theory Techn., vol. 55, no. 2, pp. 239–247, Feb. 2007.

[11] E. N. Grossman, J. E. Sauvageau, and D. G. McDonald, "Lithographic spiral antennas at short wavelengths," Appl. Phys. Lett., vol. 59, no. 25, pp.3225–3227, 1991.

[12] K. S. Saini and R. F. Bradley, "The sinuous antenna – a dual polarized element for wideband phased array feed application," Electronics Division Internal Report 301, Nat. Radio Astron. Observatory, Greenbank, WV, USA, 1996.